PCCP

Accepted Manuscript

This is an *Accepted Manuscript*, which has been through the Royal Society of Chemistry peer review process and has been accepted for publication.

Accepted Manuscripts are published online shortly after acceptance, before technical editing, formatting and proof reading. Using this free service, authors can make their results available to the community, in citable form, before we publish the edited article. We will replace this *Accepted Manuscript* with the edited and formatted *Advance Article* as soon as it is available.

You can find more information about *Accepted Manuscripts* in the Information for Authors.

Please note that technical editing may introduce minor changes to the text and/or graphics, which may alter content. The journal's standard Terms & Conditions and the Ethical guidelines still apply. In no event shall the Royal Society of Chemistry be held responsible for any errors or omissions in this *Accepted Manuscript* or any consequences arising from the use of any information it contains.

ROYAL SOCIETY OF CHEMISTRY

www.rsc.org/pccp

Journal Name

ARTICLE

Engineering the electronic and magnetic properties of d^0 2D dichalcogenide materials through vacancy doping and lattice strains

Received 00th January 20xx,
Accepted 00th January 20xx

DOI: 10.1039/x0xx00000x

www.rsc.org/

L. Ao,[a,b] A. Pham,[a*] H. Y. Xiao,[b*] X. T. Zu,[b] and S. Li[a]

Abstract: We have systematically investigated the effects of different vacancy defects in 2D d^0 materials SnS_2 and ZrS_2 using first principles calculations. The theoretical results show that single cation vacancy and vacancy complex like V-SnS6 can induce large magnetic moments ($3\mu_B$ – $4\mu_B$) in these single layer materials. Other defects, such as V-SnS3, V-S, V-ZrS3 and V-ZrS6, can result in n-type conductivity. In addition, the *ab initio* studies also reveal that the magnetic and conductive properties from the cation vacancy and defect complex V-SnS6 can be modified using the compressive/tensile strain of the in-plane lattices. Specifically, the V-Zr doped ZrS_2 monolayer, can be tuned from a ferromagnetic semiconductor to a metallic/half-metallic material with decreasing/increasing magnetic moments depending on the external compressive/tensile strains. On the other hand, the semiconducting and magnetic properties of V-Sn doped SnS_2 is preserved under different lattice compression and tension. For the defect complex like V-SnS6, only the lattice compression can tune the magnetic moments in SnS_2. As a result, by manipulating the fabrication parameters, the magnetic and conductive properties of SnS_2 and ZrS_2 can be tuned without the need of chemical doping.

1. Introduction

Single-layer dichalcogenide materials have attracted widespread attention due to their unique electronic, magnetic and optical properties. [1-8] Recently, two new members of 2D diachalcogenide materials, SnS_2 and ZrS_2, have been synthesized experimentally.[9, 10] These materials have demonstrated remarkable properties for the applications of field effect transistors, lithium ion batteries, and photodetector devices.[11-13]

Vacancy defect can have significant effect on the magnetic properties of two-dimensional (2D) materials.[14-17] For instance, transition-metal dichalcogenide material like MoS_2 grown using chemical vapor deposition (CVD) method[18] can exhibit a large magnetic moment of $6\mu_B$, which is attributed to the MoS6 vacancy complex[19]. Thus, investigating the effect of vacancy on the electronic and magnetic properties of the newly discovered SnS_2 and ZrS_2 monolayers is of great interest for future spintronic devices. Strain is another important technique that has been widely used to engineer the electronic and magnetic properties of 2D materials.[20-23] Even though the effect of lattice strain has been investigated theoretically in the pristine SnS_2 and ZrS_2,[24, 25] understanding the influence of strain on these 2D materials doped with vacancy is very limited.

In this paper, we systematically investigated the electronic and magnetic properties of vacancy-doped SnS_2 and ZrS_2 monolayers with the external lattice strain. Since both SnS_2 and ZrS_2 have the d^0 electronic configuration in the cation site, we aim to: (1) investigate if the vacancy doping can induce magnetic moments and alter the electronic properties, and (2) explore how these properties can be engineered through the strain. These results will provide an important guidance for further experimental studies of SnS_2 and ZrS_2-based magnetic devices.

2. Computational details

The spin-polarized DFT calculations were performed using the VASP code[26], with the projector augmented wave (PAW) potentials[27] and the Perdew-Burk-Ernzerhof (PBE) functional.[28] A vacuum region of 15 Å was used to avoid the interaction between the neighbouring slabs. The plane-wave basis set was expanded with a cutoff energy of 400 eV. To study the effect of vacancy doping, different types of defects were considered, such as anion S mono-vacancy (V-S), cation M (M=Sn/Zr) mono-vacancy (V-M), vacancy complex consisting of one M and its nearby three S atoms (V-MS3), and vacancy complex consisting of one M and its nearby six S atoms (V-MS6).

Different supercell sizes were employed to investigate the different vacancies' behaviours. A 4×4 supercell with a 6×6×1

[a.] *School of Material Science and Engineering, University of New South Wales, Sydney 2052, Australia*
[b.] *School of Physical Electronics, University of Electronic Science and Technology of China, Chengdu 610054, China*
E-mail: anh.pham@unsw.edu.au
† Electronic Supplementary Information (ESI) available: Supplementary Fig. S1-S3. See DOI: 10.1039/x0xx00000x

Physical Chemistry Chemical Physics Accepted Manuscript

This journal is © The Royal Society of Chemistry 20xx

Monkhorst-Pack[29] k-point mesh was used to model single cation (V-M) and anion (V-S) vacancy. For the defect complexes like V-MS3 and V-MS6, 6×6 supercells with a 4×4×1 Monkhorst-Pack k-point mesh was used for the theoretical calculations. All the atom positions were relaxed until the Hellmann-Feynman forces were less than 0.01 eV/Å. The bi-axial strain is defined as $\varepsilon\%=(c-c_0)/c_0$, where c_0 and c are the unstrained and strained lattice constants. The lattice parameters and bandgaps were calculated to be 3.69 Å and 3.63 Å, and 1.58 eV and 0.94 eV for pristine SnS_2 and ZrS_2 respectively. These values are consistent with previous theoretical and experimental results.[24, 30]

The formation energy of the vacancy doped system is given by

$$E_f=E_{V\text{-}i@MS2}-E_{MS2}+n\times\mu_M+m\times\mu_S \quad (1),$$

where $E_{V\text{-}i@MS2}$ is the total energy of the supercell containing vacancy defect, E_{MS2} is the total energy of the pristine MS_2 (M=Sn/Zr) supercell, μ_M and μ_S are the total energy of the isolated M and S atoms, respectively, and n and m are the number of M and S atoms removed from the supercell, respectively.

3. Results and discussion

3.1 Stability and structural properties of vacancy defects

To understand the stability of the vacancy doped SnS_2 and ZrS_2 monolayers, we have calculated their formation energies based on equation (1). According to Table 1, the high formation energies indicate that vacancy defects are not easy to form in both of the SnS_2 and ZrS_2 monolayers under equilibrium conditions. However, such defects can be induced in non-equilibrium processes such as e-beam lithography[31], which has been successfully applied to decorate vacancy defects in MoS_2 monolayer.[3] On the other hand, the relative low formation energies of V-S imply that single anion vacancies [Fig. 1(a)] are thermodynamically more stable in both monolayers compared to other vacancy defects [Fig. 1(b), (c), and (d)]. In addition, the formation of these defects can affect the structural geometry of the monolayers. As demonstrated in Fig. 1(d), the formation of the V-ZrS6 defect in the ZrS_2 monolayer attracts the surrounding atoms towards the vacancy site, thus enhancing the binding between the Zr and S atoms adjacent to the defects. The reconstructed structure around the vacancy now contains shorter Zr-S bonds (2.47 Å) as compared to the pristine structure (2.57 Å). However, similar vacancy complex has minimal effect on the geometry of the SnS_2 host material. Meanwhile, except for V-M, the defects, such as V-S and V-MS3 [Figs. 1(a) and (c)], introduce varying degree of distortion around the vacancy site in both materials. Specifically, the creation of anion vacancy defect repels the surrounding Zr atoms dramatically, resulting in an elongated Zr-Zr distance of 4.11 Å compared to the pristine of 3.63 Å in ZrS_2 monolayer.

Table 1 Formation energies and magnetic properties for vacancy doped SnS_2 and ZrS_2 monolayers. M_{Total}, M_S, and $M_{Sn(Zr)}$ refer to the total magnetic moment of the supercell, the magnetic moment from each first-neighboring S atom and that from each first-neighboring Sn or Zr atoms, respectively.

	E_f /eV	M_{Total} /μ_B	M_S /μ_B	$M_{Sn(Zr)}$ /μ_B
SnS_2				
V-S	5.05	0	0	0
V-Sn	9.12	4.00	0.60	0
V-SnS3	16.71	0	0	0
V-SnS6	28.34	4.00	0.40	0.20
ZrS_2				
V-S	5.76	0	0	0
V-Zr	15.53	3.05	0.45	0
V-ZrS3	24.65	0	0	0
V-ZrS6	41.14	0	0	0

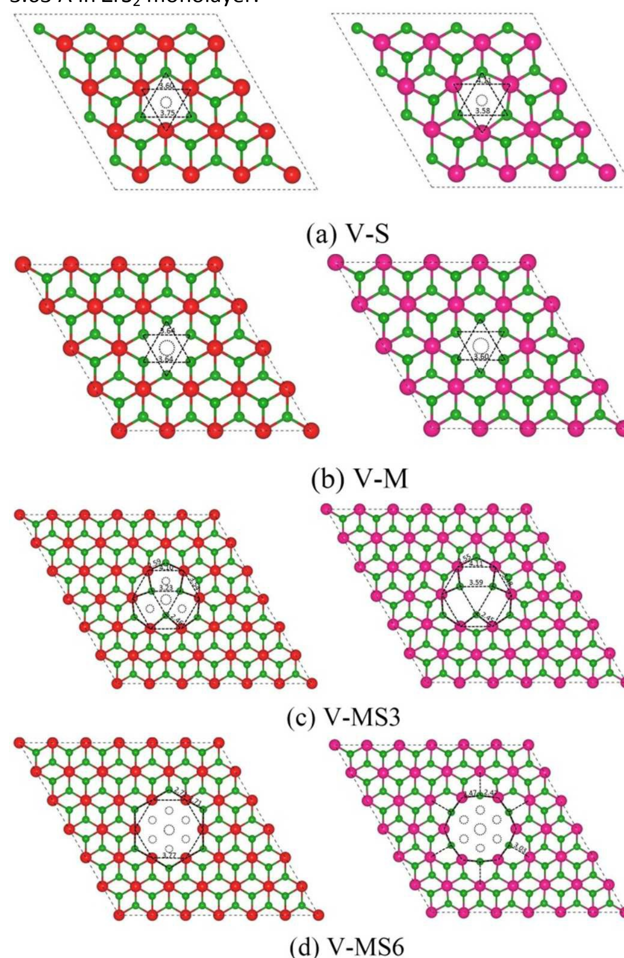

Fig. 1 Schematic view of the relaxed geometrical structure for the MS_2 (M=Sn/Zr) monolayers with (a) V-S, (b) V-M, (c) V-MS3, (d) V-MS6. Distances of the atoms near the vacancy sites are measured, which are all in angstroms. Sn, Zr, and S atoms are represented by red, pink and green balls, respectively. Dashed atoms are vacant sites.

Physical Chemistry Chemical Physics Accepted Manuscript

 This journal is © The Royal Society of Chemistry 20xx

For V-S doped SnS_2, the Sn atoms are slightly attracted towards the vacancy site, resulting in a shorter Sn-Sn distance of 3.60 Å compared to the 3.68 Å in the pristine structure. Such structural variations are attributed to the different responds of the Sn/Zr atoms to the electron redistribution. After one binding S atom is removed, the first neighbouring Zr atoms tend to find stronger bonding with the inner S atoms, leading to the decreased Zr-S bond length and the elongated Zr-Zr distance. Whereas for the Sn atoms in SnS_2, they tend to bind with each other by sharing the non-bonding electrons left in the vacancy site, resulting in the slightly decreased Sn-Sn distance.

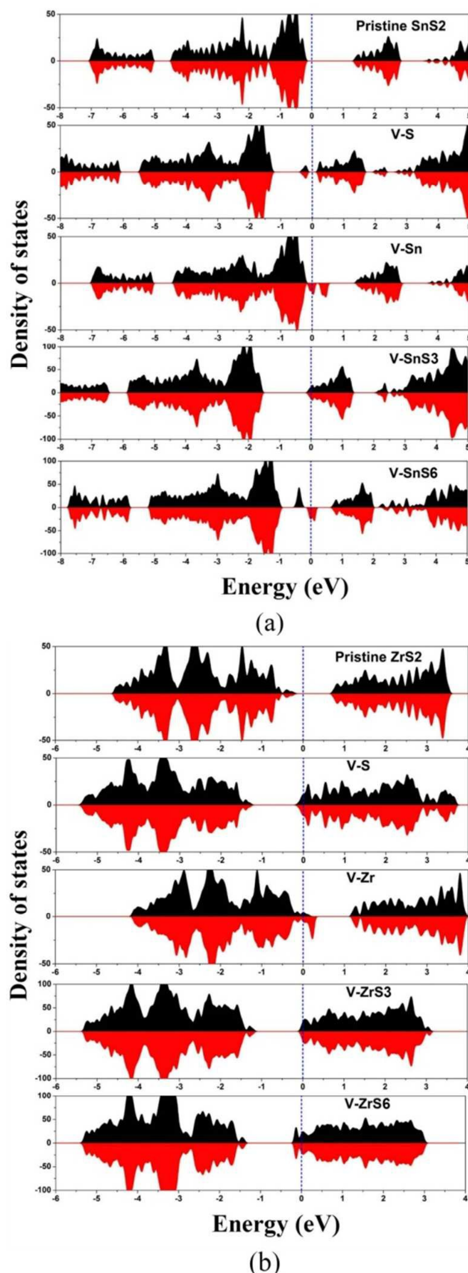

Fig. 2 The spin-resolved total density of states (DOS) for the defective (a) SnS_2 and (b) ZrS_2 monolayer. The spin up and down parts are shaded by black and red colours, respectively. The Fermi levels are set to zero, which are indicated by blue dashed lines.

3.2 Electronic and magnetic properties of vacancy defects

As demonstrated in Fig. 2, the formation of non-magnetic defects like V-S in ZrS_2 and V-MS3 in both materials shift the Fermi levels in the conduction band, indicting the effective n-type doping. In the case of V-S doped SnS_2, a defective state appears close to the bottom of the conduction band, resulting in a smaller band gap of about 0.35 eV. On the other hand, the cation vacancies induce large total magnetic moments of $4\mu_B$ and $3.05\mu_B$ in the SnS_2 and ZrS_2 monolayers, respectively. The semiconducting nature of the pristine structures is now transformed to magnetic half-metallicity and metallicity due to the delocalized S-atoms *p* states [Fig. 3(a) and (b)]. As shown in Figs. 3 and 4, such interesting electronic properties of the V-M doped MS_2 can be attributed to the holes from the cation vacancy sites, which transfer to the nearest S atoms. Bader analysis indicates that the magnetisms are mainly distributed on the six S atoms nearest the vacancy, each of which has a magnetic moment of $0.60\mu_B$ and $0.45\mu_B$ in SnS_2 and ZrS_2, respectively. The remaining magnetic moments of 0.4 μ_B and $0.35\mu_B$ are from the second neighbouring S atoms. In addition, due to the broad bandwidth of S-atoms *p* states, the magnetisms have an itinerant rather than localized character.

For the complex defects like V-MS6, the different defective monolayers exhibit contrasting magnetic and conductive properties. Specifically, V-SnS6 induces a net magnetic

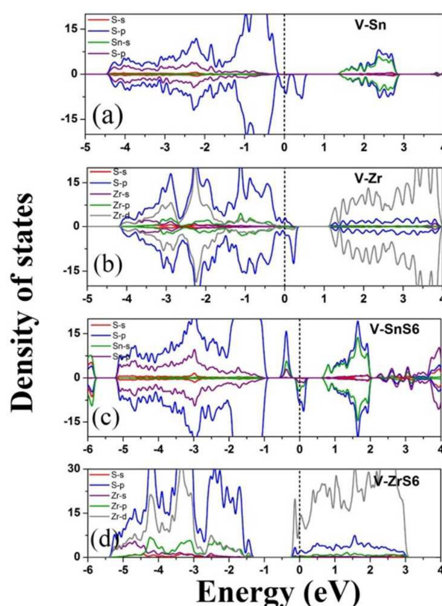

Fig. 3 Partial density of states for (a) V-Sn doped SnS_2, (b) V-Zr doped ZrS_2, (c) V-SnS6 doped SnS_2, and (d) V-ZrS6 doped ZrS_2 monolayer. The Fermi levels are all set to zero, which are indicated by black dashed line.

Physical Chemistry Chemical Physics Accepted Manuscript

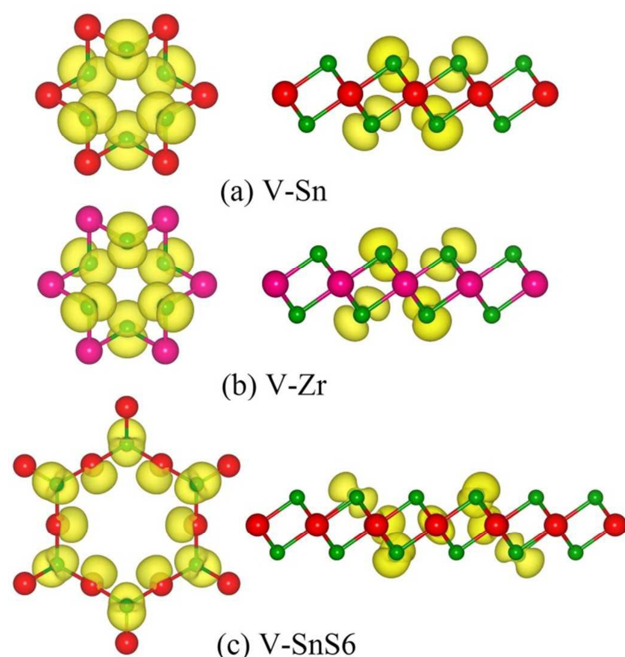

Fig. 4 Top (left) and side (right) views of the isosurface plot of the spin density for (a) V-Sn doped SnS_2, (b) V-Zr doped ZrS_2, and (c) V-SnS6 doped SnS_2 monolayer. The yellow isosurface shows the positive spin density. The isosurface value is taken as 0.003 eV/Å^3. The atoms colour coding is the same as in Fig. 1.

which are mainly distributed on the closest S and Sn atoms, as shown in Fig. 4(c). In contrast to the case of V-Sn, the spin-polarized defect states are now localized in the energy gap of the SnS_2 monolayer [Fig. 2(a)], indicating the localized magnetic moment. However, the ground state of the V-ZrS6 decorated ZrS_2 monolayer is nonmagnetic with n-type conductivity. The absence of magnetism in ZrS_2 is due to the strong distortion around the defect site, which quenches the orbital moments of S and Zr. To demonstrate the effect of structural distortion, a spin polarized calculation with fixed atom positions is conducted for the V-ZrS6 doped ZrS_2. The results show the magnetic moments of $0.77\mu_B$ and $0.11\mu_B$ on each nearby Zr and S atoms, respectively. By further examining the partial density of states [Fig. 3(d)] and the charge density difference for the V-ZrS6 doped ZrS_2 [Fig. S1 of supplementary material], it is found that the formation of such defect complex transfer 0.16 *e* to the empty Zr d orbital, making ZrS_2 n-type semiconductor.

3.3 Effects of strain on magnetic SnS_2 and ZrS_2 with vacancies

Since a single cation vacancy can induce large magnetic moments in both SnS_2 and ZrS_2, it is interesting to know how the compressive and tensile strains can influence the electronic and magnetic properties. The calculation shows that the effect of tensile strain and compression can result in different properties in SnS_2 and ZrS_2 host monolayers with the cation vacancy. As shown in Fig. 5(a), the magnetism in SnS_2 induced by V-Sn is robust against both compressive and tensile strains. It shows an average magnetic moment of $4\mu_B$ under various lattice strains, demonstrating that the strain-independent magnetic behaviour. In addition, the bandgaps of the defective SnS_2 are preserved under different lattice compression [Fig. 5(b)], with no observation of the insulator-metal transition.

For the single cation vacancy in ZrS_2, the induced magnetic moments are observed to increase and decrease with respect to the applied tensile and compressive strain, respectively. With the application of tensile strain on the in-plane lattices, the electrons from the vacancy site become more delocalized. Subsequently, they are transferred to the S atoms adjacent to the defect site as revealed in the spin density calculations as shown in Fig. 6. Further examination of the partial density of states (PDOS) of the S-atoms *p* states [Fig. S2 of supplementary material] and the band structures [Fig. 7] shows that the increasing tensile strain creates an occupied spin-states while the spin-down states are partially occupied, thus results in a half metallic ground-state. Meanwhile, applying the compressive strain results in an insulator-to-metal transition, which occurs at -8% of the compressive strain. Due to the shortened Zr-S bond lengths, moment of $4\mu_B$ in the SnS_2 host material, the delocalized S-atoms *p* states extend to Zr-atoms *d* orbital, thus resulting in a metallic character of the vacancy doped monolayer as demonstrated in Fig. 7.

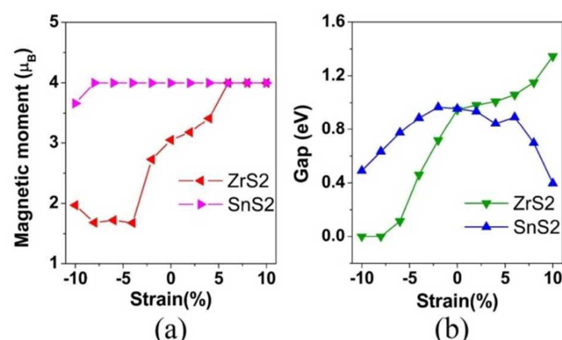

Fig. 5 Strain dependent (a) total magnetic moments and (b) band gaps for V-M doped MS_2 monolayers.

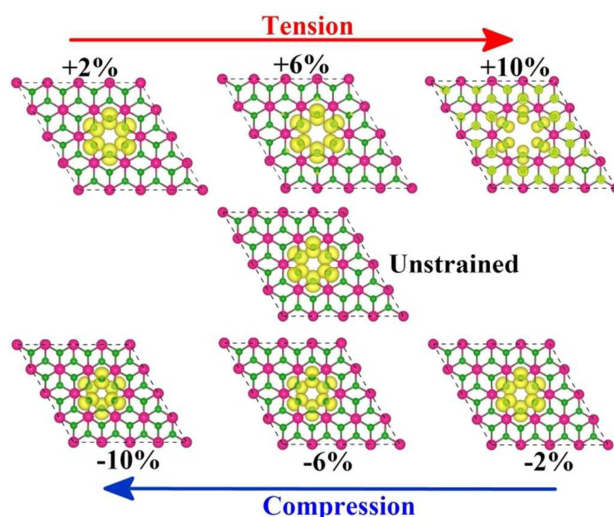

Fig. 6 Isosurfaces of the spin density for V-Zr doped ZrS_2 monolayer at both compressive and tensile strains. The isosurface value is taken as 0.003

This journal is © The Royal Society of Chemistry 20xx
Physical Chemistry Chemical Physics Accepted Manuscript

eV/Å^3. The yellow isosurface shows the positive spin density. The atoms colour coding is the same as in Fig. 1.

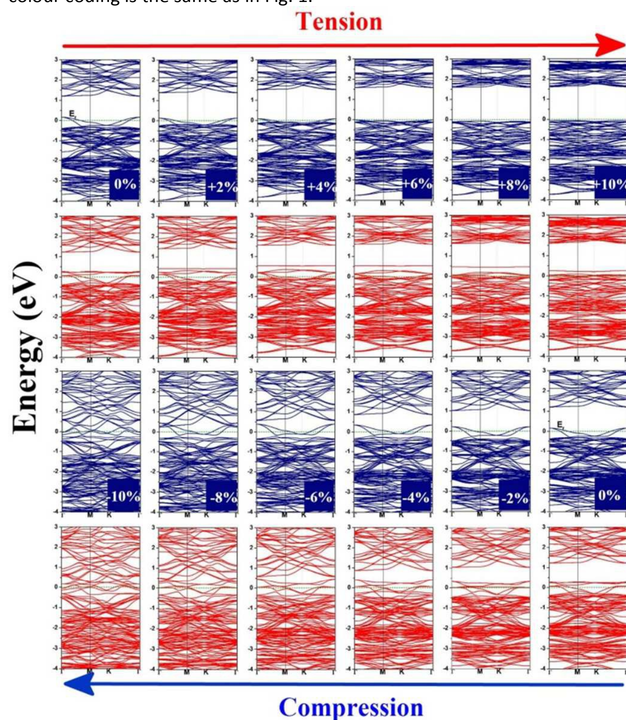

Fig. 7 Spin-polarized band structures of V-Zr doped ZrS_2 monolayer under both compressive and tensile strains. The spin-up and down parts are represented by blue and red colours, respectively. The Fermi levels are all set to zero, which are indicated by green dashed line.

In addition, the charge contours of the electronic states at 0.1 eV below the Fermi level [Fig. S3 of supplementary material] reveal that the Zr-atoms *d* states are now occupied, which are accounted for the metallic character of compressive ZrS_2.

For the defect complex V-SnS6, the tensile strain is shown to have minimal effect on the defective monolayer as demonstrated in Fig. 8. The total magnetic moments are preserved to be $4\mu_B$ with the localized character inside the bandgap. On the other hand, the electronic and magnetic properties are significantly modified under compressive strain. The total magnetic moments decrease to $2\mu_B$ when the compressive strain reaches to -4%. The decreasing total magnetic moment can be understood through the charge transfer process between the defect site and the neighbouring Sn and S sites. The charge Bader analysis reveals that the decreased magnetism is mainly due to the decreasing moments in the nearest S and Sn sites. Due to the shortened bond length of Sn-S, more charges are transferred from the defect site to the S and Sn atoms surrounding the vacancy, thus resulting in the smaller and average magnetic moments of $0.18\mu_B$ and $0.10\mu_B$, respectively. Although no semiconductor-to-metal transition occurs in our considered maximum compressive strain of -6%, the defect states are observed to move closer to the host valance band maximum along with the increasing compression.

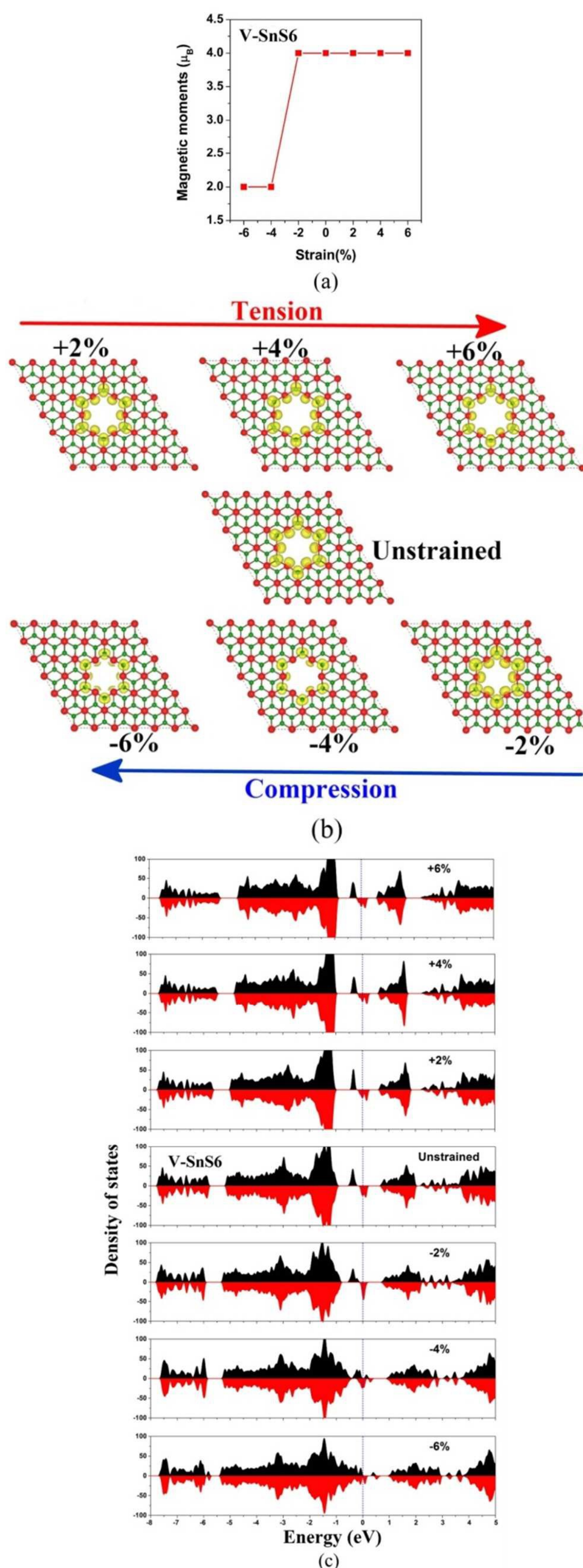

Fig. 8 Strain responses of V-SnS6 doped SnS_2 monolayer: (a) total magnetic moments; (b) isosurfaces of the spin density in which the isosurface value is taken as 0.003 eV/Å^3 and the yellow isosurface shows the positive spin density; (c) the spin-resolved DOS in which both the colour coding and the setting of fermi level are the same as in Fig. 2.

Physical Chemistry Chemical Physics Accepted Manuscript

4. Conclusions

In conclusion, we have systematically investigated the effect of cation, anion vacancy and vacancy complex defects in SnS_2 and ZrS_2 on the electronic and magnetic properties with the applied lattice strain. The results demonstrate that defects, such as V-Sn, V-Zr and V-SnS6, can induce magnetic ground state in these monolayers. Effective n-type doping can be achieved by the creation of V-SnS3 in SnS_2 and V-S, V-ZrS3, V-ZrS6 in ZrS_2. In addition, the lattice strain can have different effects on SnS_2 and ZrS_2 decorated with the different vacancies. SnS_2 monolayer decorated with vacancy complex of V-SnS6 is sensitive to the compressive strain but robust against tensile strain. While both tensile and compressive lattice strain can effectively modulate the electronic and magnetic properties of V-Zr doped ZrS_2, V-Sn doped SnS_2 exhibits robust magnetism against strains. These different magnetic and electronic ground states are due to the nature of the different orbital contribution of the cation in the band structure. For ZrS_2 with V-Zr, lattice compression results in the occupation of the host empty d bands, inducing the insulator-to-metal transition. In addition, the lattice compression also tune the charge transfer process between the defect sites and the neighboring S atoms in ZrS_2 with V-Zr, and Sn/S sites in SnS_2 with V-SnS6, resulting in the reduction of total magnetic moments. On the other hand, tensile strain changes V-Zr doped ZrS_2 to a half metallic magnetic material due to the occupied *p*-orbital in the S sites. Consequently, through a combination of strain tuning and defect decorating, the magnetic and conductive properties can be engineered in these 2D d^0 materials for spintronic devices.

Acknowledgements

This work was supported by the NSAF Joint Foundation of China (Grant No. U1330103), the National Natural Science Foundation of China (Grant No. 51201026), the Fundamental Research Funds for the Central Universities of China (Grant No. ZYGX2011J038), and Prof. Xiao Liu's Scientific Research Starting Funding of Young Qianren Plan (A10002010401005). H.Y. Xiao acknowledges the Scientific Research Starting Funding of University of Electronic Science and Technology of China (Grant No. Y02002010401085). A. Pham and S. Li would like to thank the financial support by Australian Research Council Discovery Program of DP150103006 and DP140104373. The theoretical calculations were performed using the supercomputer resources at the National Supercomputer Center in Tianjin and the National Computing Infrastructure in Australia.

References

1 S. Horzum, D. C¸akır, J. Suh, S. Tongay, Y. S. Huang, C. H. Ho, J. Wu, H. Sahin and F. M. Peeters, *Phy. Rev. B*, 2014, **89**, 155433.
2 Y. G. Zhou, Z. G. Wang, P. Yang, X. T. Zu, L. Yang, X. Sun and F. Gao, *ACS Nano*, 2012, **6**, 9727.
3 H. P. Komsa, J. Kotakoski, S. Kurasch, O. Lehtinen, U. Kaiser and A. V. Krasheninnikov, *Phy. Rev. Lett.*, 2012, **109**, 035503.
4 J. G. Carmen, P. Anh, Y. Aibing and L. Sean, *Journal of Physics: Condensed Matter*, 2014, **26**, 306004.
5 R. Mishra, W. Zhou, S. J. Pennycook, S. T. Pantelides and J. C. Idrobo, *Phy. Rev. B* 2013, **88**, 144409.
6 D. J. Late , B. Liu, J. J. Luo, A. M. Yan, H. S. S. R. Matte , M. Grayson, C. N. R. Rao and V. P. Dravid, *Adv. Mater.* , 2012, **24**, 3549.
7 Y. Ma, Y. Dai, M. Guo, C. Niu, Y. Zhu and B. Huang, *ACS Nano*, 2012, **6**, 1695-1701.
8 A. Splendiani, L. Sun, Y. Zhang, T. Li, J. Kim, C.-Y. Chim, G. Galli and F. Wang, *Nano Letters*, 2010, **10**, 1271-1275.
9 Y. Wen, Y. Zhu and S. Zhang, *RSC Advances*, 2015, **5**, 66082-66085.
10 G. Su, V. G. Hadjiev, P. E. Loya, J. Zhang, S. Lei, S. Maharjan, P. Dong, P. M. Ajayan, J. Lou and H. Peng, *Nano Letters*, 2015, **15**, 506-513.
11 M. Zhang, Y. Zhu, X. Wang, Q. Feng, S. Qiao, W. Wen, Y. Chen, M. Cui, J. Zhang, C. Cai and L. Xie, *Journal of the American Chemical Society*, 2015, **137**, 7051-7054.
12 Z. Liu, H. Deng and P. P. Mukherjee, *Acs Applied Materials & Interfaces*, 2015, **7**, 4000-4009.
13 Y. Tao, X. Wu, W. Wang and J. Wang, *Journal of Materials Chemistry C*, 2015, **3**, 1347-1353.
14 Y. D. Ma, Y. Dai, M. Guo, C. W. Niu, J. B. Lua and B. B. Huang, *Phys. Chem. Chem. Phys.*, 2011, **13**, 15546.
15 O. V. Yazyev and L. Helm, *Phy. Rev. B*, 2007, **75**, 125408.
16 M. S. Si and D. S. Xue, *Phy. Rev. B*, 2007, **75**, 193409.
17 L. Ao, H. Y. Xiao, X. Xiang, S. Li, K. Z. Liu, H. Huang and X. T. Zu, *Physical Chemistry Chemical Physics*, 2015, **17**, 10737-10748.
18 W. Zhou, X. L. Zou, S. Najmaei, Z. Liu, Y. M. Shi, J. Kong, J. Lou, P. M. Ajayan, B. I. Yakobson and J. C. Idrobo, *Nano Lett.*, 2013, **13**, 2615-2622.
19 H. L. Zheng, B. S. Yang, D. D. Wang, R. L. Han, X. B. Du and Y. Yan, *App. Phy. Lett.*, 2014, **104**, 132403
20 B. Ouyang and J. Song, *App. Phy. Lett.* , 2013, **103**, 102401.
21 W. S. Yun and J. D. Lee, *Journal of Physical Chemistry C*, 2015, **119**, 2822-2827.
22 N. Lu, H. Guo, L. Li, J. Dai, L. Wang, W.-N. Mei, X. Wu and X. C. Zeng, *Nanoscale*, 2014, **6**, 2879-2886.
23 P. Johari and V. B. Shenoy, *Acs Nano*, 2012, **6**, 5449-5456.
24 Y. Li, J. Kang and J. Li, *Rsc Advances*, 2014, **4**, 7396-7401.
25 D. M. Guzman and A. Strachan, *Journal of Applied Physics*, 2014, **115**, 243701.
26 G. Kresse and J. Furthmuller, *Phys. Rev. B*, 1996, **54**, 11169.
27 P. E. Blöchl, *Phys. Rev. B*, 1994, **50**, 17953.
28 J. P. Perdew, K. Burke and M. Ernzerhof, *Phys. Rev. Lett.* , 1996, **77**, 3865.
29 H. J. Monkhorst and J. D. Pack, *Phys. Rev. B*, 1976, **13**, 5188.
30 C. Xia, Y. Peng, H. Zhang, T. Wang, S. Wei and Y. Jia, *Physical Chemistry Chemical Physics*, 2014, **16**, 19674-19680.
31 J. M. Gibson, *Phys. Today*, 1997, **50**, 56.

Physical Chemistry Chemical Physics Accepted Manuscript

This journal is © The Royal Society of Chemistry 20xx